Mechanistic modelling of the large-scale Lassa fever epidemics in Nigeria from 2016 to 2019

Salihu S. Musa[1,2], Shi Zhao[3,4,5], Daozhou Gao[6], Qianying Lin[1,7],
Gerardo Chowell[8,9] & Daihai He[1,*]

1 Department of Applied Mathematics, The Hong Kong Polytechnic University, Hong Kong

2 Department of Mathematics, Kano University of Science and Technology, Wudil, Nigeria

3 School of Nursing, The Hong Kong Polytechnic University, Hong Kong

4 JC School of Public Health and Primary Care, Chinese University of Hong Kong, Hong Kong

5 Shenzhen Research Institute of Chinese University of Hong Kong, Shenzhen, China

6 Mathematics and Science College, Shanghai Normal University, Shanghai, China

7 Michigan Institute for Data Science, University of Michigan, Ann Arbor, MI, USA

8 School of Public Health, Georgia State University, Atlanta, GA, USA

9 Fogarty International Center, National Institute of Health, Bethesda, MD, USA

∗ Correspondence to: daihai.he@polyu.edu.hk (DH)

February 26, 2020

Abstract

Lassa fever, also known as Lassa hemorrhagic fever, is a virus that has generated recurrent outbreaks in West Africa. We use mechanistic modelling to study the Lassa fever epidemics in Nigeria from 2016-19. Our model describes the interaction between human and rodent populations with the consideration of quarantine, isolation and hospitalization processes. Our model supports the phenomenon of forward bifurcation where the stability between disease-free equilibrium and endemic equilibrium exchanges. Moreover, our model captures well the incidence curves from surveillance data. In particular, our model is able to reconstruct the periodic rodent and human forces of infection. Furthermore, we suggest that the three major epidemics from 2016-19 can be modelled by properly characterizing the rodent (or human) force of infection while the estimated human force of infection also present similar patterns across outbreaks. Our results suggest that the initial susceptibility likely increased across the three outbreaks from 2016-19. Our results highlight the similarity of the transmission dynamics driving three major Lassa fever outbreaks in the endemic areas.

Keywords: Lassa fever, mathematical modelling, stability analysis, data fitting.

1

1 Introduction

Lassa fever, also known as the Lassa hemorrhagic fever (LHF), is an acute viral hemorrhagic illness that lasts 2-21 days in humans and generated recurrent outbreaks in West Africa [4, 23, 55, 68]. The Lassa virus is an *arenavirus*, from the family of *arenaviradae*, that is mainly transmitted to humans through direct contact with food or household items contaminated with urine or stools from infected rodents [5, 28, 68, 69]. The human-to-human and laboratory transmissions could also be possible [28, 68]. Thus, LHF is largely a zoonotic disease, i.e., humans become infected when in contact with an infected animal [23, 54]. The disease is endemic in West Africa where the LHF risk areas approximately cover 80% of Sierra Leon and Liberia, 50% of Guinea, 40% of Nigeria, 30% of Benin, Cote d'Ivoire and Togo and 10% of Ghana [3, 23]. Regarding its severity, it is life-threatening with an estimated 2-3 million cases and 5000-10000 deaths annually [23, 52, 54]. Since its discovery in 1969 in the village known as Lassa in Borno state of northern Nigeria [28, 40, 54, 55], nosocomial outbreaks of LHF occurs repeatedly in Liberia, Nigeria and Sierra Leone [6, 8, 10, 23, 24, 38, 54].

The animal host (reservoir) of LHF virus is a rodent of the genus *Mastomys natalensis* called the *multimammate* rat which was found to be first infected with the virus in Nigeria and in Sierra Leon in 1972, and Guinea in 2006 [15, 22, 23, 21, 28, 39]. The infected rats do not become ill but they can shed the virus through their urine and stools [23, 54, 68]. About 80% of individuals infected with LHF virus do not show symptoms [68] while about 1 in every 5 symptomatic infections result in severe cases in which numerous organs such as kidney, liver, spleen are affected [68]. Reinfection can occur for LHF [43, 44], even though more clinical evidence is needed for this assertion [44]. According to previous studies, the LHF prevalence is amplified in the rainy season as rainfall influences rodent migration from its natural habitat to human environment in order to breed and gain propinquity during the dry season (and at the beginning of the rainy season) during which the rodent-human contact rate increases, enhancing the risk of exposure to LHF [3, 4, 16, 22, 23, 39, 46, 56, 63]. Previous studies reveal that rainfall plays an essential role (a key ecological factor) for the transmission of LHF, because the attack rate was 2-3 times higher in the rainy season than in the dry season [22, 23]. Symptoms associated with LHF include fever, headache, general weakness and malaise, muscle pain, sore throat, nausea, chest pain, cough, vomiting, diarrhoea, and abdominal pain [68]. In severe cases, fluid in the lung cavity, facial swelling, bleeding from the nose, mouth, vagina or gastrointestinal tract and low blood pressure may develop [4, 68]. In fatal cases, death usually occurs two weeks after the onset of the symptoms [68]. Lost of hearing may also occur after recovery [55].

Currently, there is no vaccine available against LHF. However, the antiviral drug ribavirin appears to be an effective treatment if administered early in the course of clinical illness [23, 54, 68]. Control of the rodent population has been largely unfeasible, therefore, measures frequently focus on keeping rats out of home and food items [68]. Further, there is evidence of vertical transmission in the rodent population [21], and the vertical transmission rate could be higher during the rainy season when the rodents are more involved in patrolling their houses for mating and breeding [21].

Various mathematical models have been developed to investigate the transmission dynamics of LHF [3, 37, 58, 51, 54, 70]. Some of which focused on the study of theoretical modelling analysis reveal dynamical features of LHF transmission within human and rodent (as a reservoir) populations. Saez *et al.* [58] found that chemical treatment intervention is the key control measure to reduce the rodent population, which in turn reduces LHF infection. Akhmetzhanov *et al.* [3] developed a mathematical model to explore the transmission dynamics of LHF in rodent population and the impact to human cases, while quantifying the major seasonal factors for the LHF infection, and found that seasonal migration of the rodent populations plays a significant role in seasonal transmission of the LHF. James *et al.* [37] proposed a deterministic model of LHF transmission dynamics and incorporated

quarantine in an infectious class of humans. Onuorah *et al.* [54] developed a mathematical model for the transmission dynamics of LHF, and found that the basic reproduction ratio is most sensitive to human birth rate followed by condom efficacy and compliance. Obabiyi and Akindele [51] designed a compartmental model to describe the transmission dynamics of the LHF within humans and reservoir populations. Their results suggested that early diagnosis of infected human cases, maintaining hygienic environment, enhanced infection control in hospitals, and controlling the population of the rodent population carrying the virus are the best strategies to mitigate the spread of the virus.

In this paper, we will extend previous studies [3, 58, 37, 54, 51] by incorporating quarantine or isolation and hospitalization of infected individuals to better understand the transmission dynamics of the LHF epidemics. We also incorporate different types of transmission routes, i.e., human-to-human, rodent-to-human, human-to-rodent, and rodent-to-rodent. Note that rodent-to-human and human-to-rodent may be regarded as one transmission route, which is similar to the vectorial transmission for mosquito-borne diseases). In addition, this paper considers both standard incidence and mass action incidence rates and, to the best of our knowledge, it is the first time to simultaneously include the two incidence functions in modelling the transmission dynamics of the LHF. We also fit our model to the real data to show the patterns of the LHF epidemics from 2016 to 2019 in Nigeria. Our results contribute to a better understanding of the LHF epidemics and highlight some useful control measures to future LHF outbreaks. Further, we use the center manifold theory to analyze the existence of the forward bifurcation that the associated disease-free equilibrium (DFE) and the endemic equilibrium (EE) exchanges stability at $\mathcal{R}_0 = 1$ and the detailed analysis can be found in Appendix A1. Finally, sensitivity analysis, and sub-exponential growth fitting of the initial growth phases of the epidemics are also given in Appendices A2 and A3, respectively.

2 Methods

2.1 Lassa fever cases data

The time series data of LHF confirmed cases were obtained from the Nigeria Centre for Disease Control (NCDC) disease surveillance report [50] from 2016 to 2019, and we focus our analysis on the first 30 weeks of each year. Because these time interval covers the dry season (during which the rodent-human contact rate increases which enhance the risk of exposure to LHF) and the beginning of the rainy season (since rainfall influences rodent migration from its natural habitat to human environment which increases the rate of LHF transmission) in Nigeria [3, 4, 16, 22, 23, 39, 46, 56, 63]. Further, the LHF epidemics appear to be higher in the first 30 weeks of each year (i.e. 2016-19), since the population size of rodent is time dependent (low in Oct to Feb, high in Mar to May) [50].

2.2 Epidemic model

We split the total human population at time t, denoted by $N_h(t)$, into sub-populations of non-quarantined susceptible, $S_h(t)$, non-quarantined latently-infected (latently-infected means those that are infected but not yet show clinical symptoms of the disease), $E_h(t)$, quarantined latently-infected, $E_q(t)$, non-quarantined symptomatically infected, $I_h(t)$, quarantined symptomatically infected, $I_q(t)$, hospitalized, $H(t)$ and recovered, $R_h(t)$, individuals, so that

$$N_h(t) = S_h(t) + E_h(t) + I_h(t) + E_q(t) + I_q(t) + H(t) + R_h(t).$$

The total rodent (reservoir) population at time t, represented by $N_r(t)$, is split into two compartments of susceptible and infected rodents. Hence, we have
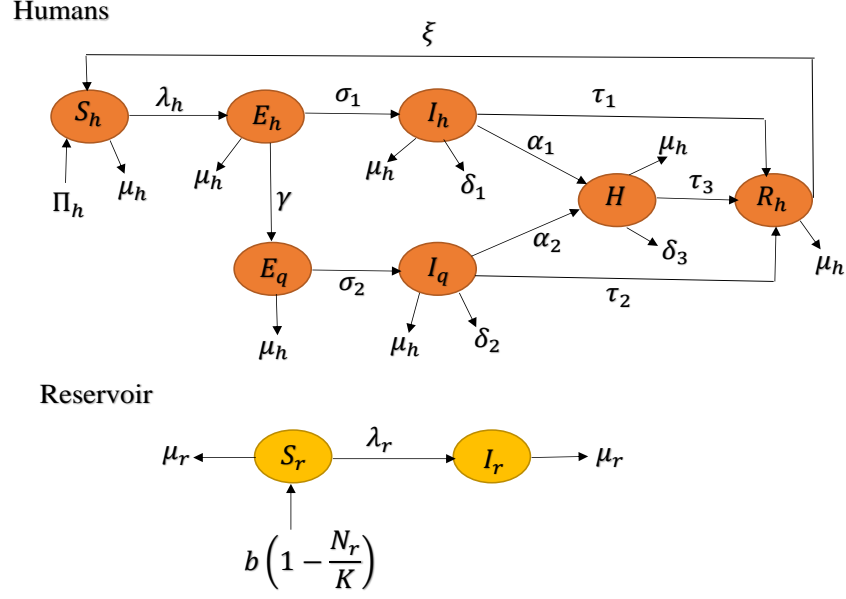
$$N_r(t) = S_r(t) + I_r(t).$$

Figure 1: Schematic diagram of the model (2.1).

The LHF model presented in Fig. 1, the state variables in Table 1, and the parameters in Table 2 (all the parameters are assumed to be positive) satisfy the following system of non-linear ordinary differential equations,

$$\frac{\mathrm{d}S_h}{\mathrm{d}t} = \Pi_h + \xi R_h - \lambda_h S_h - \mu_h S_h,$$

$$\frac{\mathrm{d}E_h}{\mathrm{d}t} = \lambda_h S_h - (\sigma_1 + \gamma + \mu_h)E_h,$$

$$\frac{\mathrm{d}I_h}{\mathrm{d}t} = \sigma_1 E_h - (\tau_1 + \alpha_1 + \delta_1 + \mu_h)I_h,$$

$$\frac{\mathrm{d}E_q}{\mathrm{d}t} = \gamma E_h - (\sigma_2 + \mu_h)E_q,$$

$$\frac{\mathrm{d}I_q}{\mathrm{d}t} = \sigma_2 E_q - (\tau_2 + \alpha_2 + \delta_2 + \mu_h)I_q, \qquad (2.1)$$

$$\frac{\mathrm{d}H}{\mathrm{d}t} = \alpha_1 I_h + \alpha_2 I_q - (\tau_3 + \delta_3 + \mu_h)H,$$

$$\frac{\mathrm{d}R_h}{\mathrm{d}t} = \tau_1 I_h + \tau_2 I_q + \tau_3 H - (\xi + \mu_h)R_h,$$

$$\frac{\mathrm{d}S_r}{\mathrm{d}t} = b\left(1 - \frac{N_r}{K}\right)N_r - \lambda_r S_r - \mu_r S_r,$$

$$\frac{\mathrm{d}I_r}{\mathrm{d}t} = \lambda_r S_r - \mu_r I_r.$$

Here, the forces of infection for humans and rodents are respectively given by

$$\lambda_h = \lambda_{hh} + \lambda_{hr} \quad \text{and} \quad \lambda_r = \lambda_{rr} + \lambda_{rh}, \qquad (2.2)$$

where
$\lambda_{hh} = \frac{\beta_1 I_h + \beta_2 I_q + \beta_3 H}{N_h}$, $\lambda_{hr} = \beta_4 I_r$, $\lambda_{rh} = \beta_5 I_h + \beta_6 I_q + \beta_7 H$, and $\lambda_{rr} = \frac{\beta_8 I_r}{N_r}$ represent human-to-human transmission, rodent-to-human transmission, human-to-rodent transmission, and rodent-to-rodent transmission, respectively.

The Lassa induced death rate satisfies the inequality $\delta_1 > \delta_2 > \delta_3$, indicating that the death induced by the LHF is higher in the I_h class than I_q class, followed by the H class. This may be due to the impact of health care and treatment for quarantined and hospitalized people. We further assume that the susceptible rodent population follows a logistic growth rate, given by, $b(1 - \frac{N_r}{K})$ [17].

The basic reproduction number is calculated using the next generation matrix technique, which represents the number of secondary cases that one infected individual would reproduce if the person is placed into a completely susceptible population [19, 47, 67]. The bifurcation analysis is performed by using Center Manifold Theory as presented in Castillo-Chavez and Song [12]. Detailed mathematical analyses of the model (2.1) can be found in Appendix A1.

The number of cases of the i-th week is

$$Z_i = \int_{\text{week } i} \rho^*(\tau_3 + \delta_3 + \mu_H)H \, \mathrm{d}t, \qquad (2.3)$$

where ρ^* denotes a constant reporting rate of the LHF cases.

2.3 Fitting framework

We model the reported LHF cases, C_i for the i-th week during the study period, as a partially observed Markov process (POMP, also known as hidden Markov model, HMM). Instead of

Table 1: Description of the state variables of the model (2.1).

Variable	Description
N_h	Total population of humans
S_h	Susceptible humans with risk of LHF infection
E_h	Non-quarantined humans exposed to LHF infection
I_h	Non-quarantined infected humans with symptoms of LHF infection
E_q	Quarantined exposed humans
I_q	Quarantined infected humans
H	Hospitalized humans
R_h	Recovered humans
N_r	Total population of rodents
S_r	Susceptible rodents
I_r	LHF infected rodents

Table 2: Description of parameters of the model (2.1).

Parameter	Interpretation/Description
Π_h	Recruitment rate for humans
μ_h, μ_r	Natural death rates of humans and rodents respectively
$\beta_i(i = 1, 2, ..., 8)$	Transmission rates
σ_1	Progression rate from E_h to I_h
σ_2	Progression rate from E_q to I_q
$\tau_i(i = 1, 2, 3)$	Recovery rates
$\alpha_l(l = 1, 2)$	Hospitalization rates
γ	Rate of quarantine from E_h to E_q
ξ	Rate of relapse from R_h to S_h
K	Maximal carrying capacity of rodents
b	Maximum growth rate of the rodents
$\delta_i(i = 1, 2, 3)$	Disease-induced death rates for humans

implementing Poisson-distributed priors [72], all C_i's are assumed to follow over-dispersed Poisson distributions according to the theoretical modelling (Eqn (2.3)) outputs, Z_is. Since the rate of Poisson distribution is a Gamma random variable, the observed weekly number of people who are confirmed LHF cases (C_i of the i-th week) is a random sample from a negative-binomial (NB) distribution. Therefore, for each (or a single) year,

$$C_i \sim \text{NB}(\text{mean} = Z_i, \text{variance} = Z_i(1 + \tau Z_i)), \tag{2.4}$$

where τ (> 0) is an over-dispersion parameter for NB distribution to be estimated. In this likelihood framework, we set $L_{i,j}(\cdot)$ be the likelihood function for the i-th week of the j-th year, which is the probability measurement of the observed number of cases, given the real cases from simulations Z_i under the NB distribution in Eqn (2.4) [7, 42]. The R (version 3.4.1) package "POMP" [64] was used for the model calibration.

The overall log-likelihood, l, for the whole time series is

$$l(\Theta) = \sum_{j=1}^{3} \sum_{i=1}^{T} \ln[L_{i,j}(C_{i,j} \mid C_{0,j}, ..., C_{i-1,j}; \Theta)]. \tag{2.5}$$

Here, Θ is the parameter vector under estimation, and T represents the total number of weeks in a wave (in this work we only focus on the first 30 weeks in each wave and five parameters were estimated). To express the $l(\Theta)$ in this form it is convenient to simulate with an identical transmission rate for the three waves.

We employed the iterated filtering algorithm with the plug-and-play likelihood-based inference framework to estimate the maximum likelihood estimates (MLE) of Θ ([9, 20, 29, 31, 32, 34, 35, 42]. We used the fixed-time-step Euler-multinomial algorithm to simulate the ODE system (2.1). Model performance is compared by using the small-sample-size corrected Akaike's Information Criterion (AICc) [9]. The AICc is a measurement of the trade-off between the model complexity and the goodness-of-fit. The AICc is given by

$$\text{AICc} = -2l\left(\hat{\Theta}\right) + 2k + \frac{2M(M+1)}{N-M-1}. \tag{2.6}$$

Here, N is the number of data points, i.e., sample size, and M represents the number of parameters to be estimated.

To illustrate that the model (2.1) can be used to describe the epidemics of LHF in Nigeria, we fit the model (with most parameter values given) to the 30 weeks of data for each of 2016, 2017, and 2018. The epidemics in 2016, 2017 and 2018 share strikingly similar patterns, but the magnitude is increasing by a factor of (roughly) two every year. The similar patterns in the data suggest that the driving force (from rodent) of the LHF epidemic could have similar pattern across years, or could be completely periodic or differ only by a factor.

We assumed that an infection from rodent to human is time-dependent and should be possible to synthesize all rodent contributed infection (to human) as one time-dependent function. Using the cubic spline numerical approach to fit the LHF epidemic data and reconstruct the Z_i series [30, 73].

We let n_z to represent the number of nodes in the cubic spline of $\lambda_h(t)$. Different possible values of n_z's were tested to examine the value that could give lowest AICs. In addition, we suggested that the 2016-2019 LHF epidemics share similar cubic spline function of $\lambda_h(t)$, although we observed that the seasonal trends of the LHF epidemics might be increasing over a certain period of time.

2.4 Two fitting schemes

We fit the model (2.1) to the weekly time series data on LHF cases of three major outbreaks in Nigeria during 2016-19 to explore the LHF transmission dynamics. We conducted the fitting with two schemes (each with five parameters estimated) and included several biologically reasonable simplifications in the fitting.

By fitting the epidemic model to the real-world time series data on LHF cases, we aim to reconstruct the time-varying transmission rates or forces of infection (FoIs).

2.4.1 Scheme I

In model (2.1), the transmission paths are controlled by the effective contact parameters, i.e., β_1-β_8. The β_4 and β_8 are the effective "contact" rate from rodents to humans and to rodents, respectively.

Thus, both $\beta_4(t)$ and $\beta_8(t)$ attribute to the rodents contributed transmission effects. The remaining contact parameters, i.e., β_1, β_2, β_3, β_5, β_6 and β_7, are the humans contributed transmission effects. In scheme I, we assumed all the rodents contributed transmission to be time-varying, and all humans contributed transmission to be constant over the study period.

In the preliminary fitting, we attempted two scenarios: (i) $\beta_4(t) \neq \beta_8(t)$, the two rodents contributed transmission paths determined by different time-varying functions, and (ii) $\beta_4(t) = \beta_8(t)$, the two rodents contributed transmission paths to be the same time-varying function. The preliminary fitting results showed that relaxing the scenario, i.e., changing from scenario (ii) to (i), does not improve the model in term of AICc. The likelihood ratio (LR) test yields a consistent outcome that the scenario (i) fails to improve the model performance significantly. Therefore, for simplicity, scenario (ii), is presumed and adopted in this scheme.

Although human contributed β_1, β_2, β_3, β_5, β_6 and β_7 are not necessarily equal in the model (2.1), we set $\beta_1 = \beta_2 = \beta_3$ and $\beta_5 = \beta_6 = \beta_7$ in the fitting. This is another simplification based on the fact that most of LHF cases would not be effectively quarantined nor hospitalized, and thus they could be as infectious as the cases in the general population.

2.4.2 Scheme II

Previous studies show that the great majority of LHF cases result from the transmission from rodents to humans [23, 36, 68]. Based on this fact, the similar qualitative patterns in the LHF epidemics across years stimulate us to presume that the rodents-driven transmission path, i.e., λ_r in the model (2.1), of the epidemic could have the same pattern. In contrast, the force of infection (FoI) driven by humans, λ_h, could present different shape across years. The two FoI's, λ_r and λ_h, are considered to be time-varying and are reconstructed by using the cubic spline function. We model all rodent contributed infections by one time-varying FoI, $\lambda_r(t)$. Each epidemic curve is fitted with the same reconstructed $\lambda_r(t)$ but different $\lambda_h(t)$. In other words, the λ_r's are assumed to be the same in each year, however, the λ_h could vary across years.

3 Results

The fitting results under scheme I (section 2.4.1) were shown in Fig 2. Our LHF epidemic model elucidates similar temporal patterns of the LHF transmission dynamics in Nigeria from 2016-19 under biologically reasonable conditions. Fig. 2 shows the dynamics of the rodent population by incorporating a time-dependent rodent population size, although the information on LHF prevalence among rodent is still insufficient. It reveals that the outbreak of LHF among rodents appears to be in the first half of each year. Therefore, the observed human outbreaks result from an outbreak among rodents plus a time-dependent (basically a step-function type) transmission rate from rodent to human (or spill-over rate). The parameter $\beta_4(t)$, which is time-varying, takes the maximum value from Nov to Feb of every year, after which the value drops to a minimum. Our fitting result provides a possible mechanism for understanding the annual outbreaks of LHF. The increasing amplitude of LHF could be explained by higher initial/baseline infectious human cases in November 2017 and 2018 than in November 2016. We assumed the transmission rates to be identical across the three outbreaks. The higher initial infectious human cases could be due to higher rainfall in 2017 and 2018 than in 2016, even though there could be other possible mechanisms such as differential impact of prevention efforts and behavior changes.
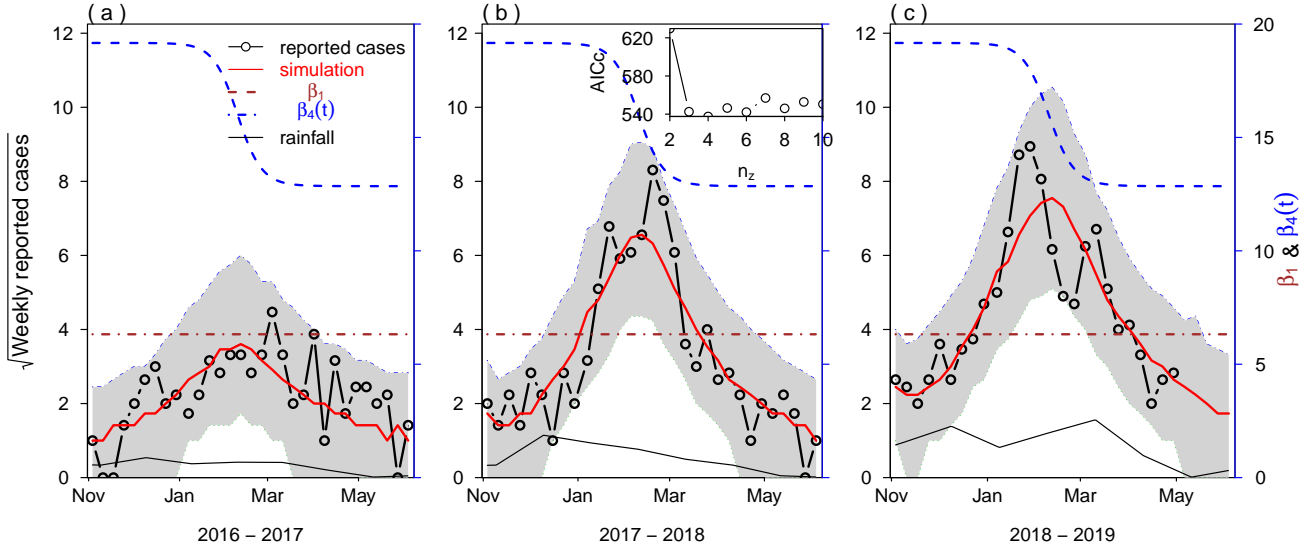
Figure 2: Fitting transmission rates of the model (2.1) by using the cubic spline function for scheme I. The black circles are the observed numbers of LHF cases, and the red solid line are the simulation medians. The grey shaded regions represent the 95% CIs from the simulation. The black curve (thick line) represents the daily rainfall with delay of 145 days. The blue dashed line represents the transmission rate from rodents to humans, β_4; and the brown dashed-dotted line represents the human-to-human transmission rate, β_1. The parameter estimates are summarized in Table 3. The inset panel in (b) shows the AICc as a function of n_z, the number of nodes in the cubic spline. Since $n_z = 4$ attains the minimum AICc, thus $n_z = 4$ was used in (a-c).

The fitting results under scheme II (section 2.4.2) were shown in Fig 3. The rodents FoI (λ_r), the average prevalence rates (infection rates) of λ_h, and the temporal pattern of the $\lambda_r(t)$ are shown in Fig 3. We found that the LHF epidemics can be reconstructed by the same FoI from rodents (λ_r) together with similar FoI from humans (λ_h). Our model (2.1) is able to capture the observed LHF epidemics for the three years with synchronized λ_r. The synchronization of λ_r across years indicates the strong seasonality in the rodent-driven FoI is perfectly in-phase. Although λ_h's are assumed to be fully flexible (i.e., different) from 2016-19, the reconstructed λ_h's appear to have a similar pattern (i.e., seasonality) in each year.

Given the same λ_r for each year, though λ_h's appear to have a similar pattern across years, it is neither perfectly in-phase nor with the same scale. Although we show that the estimated FoI's exhibit similar seasonal trends in 2016-2019, not all of them were synchronized in each case despite their proximity. These results also can be extended on the LHF transmissibility in terms of the effective reproduction number, denoted by $\mathcal{R}_{\text{eff}}$. Note that $\mathcal{R}_{\text{eff}} = \mathcal{R}_0 s_h(0)$, where $\mathcal{R}_0$ is the basic reproduction number and $s_h(0)$ (ranges from 0 to 1) is the percentage of population which is susceptible at the initial stage of the outbreak. The initial susceptibility $s_h(0)$ at the beginning of each year are estimated to increase across years. Note that the infection rate of the cases in terms of the standard "SIR" model is defined by the product of the effective transmission rate (β), population susceptibility (S_h) and infectivity (I_r), i.e., "$\beta S_h I_r$". Although we have restricted the major FoI (i.e., λ_r) to be the same across years for the fitting simplicity, it is more likely to be variable in practice. Thus, the estimated increase in the $s_h(0)$ actually reflects increase in the case prevalence rate across
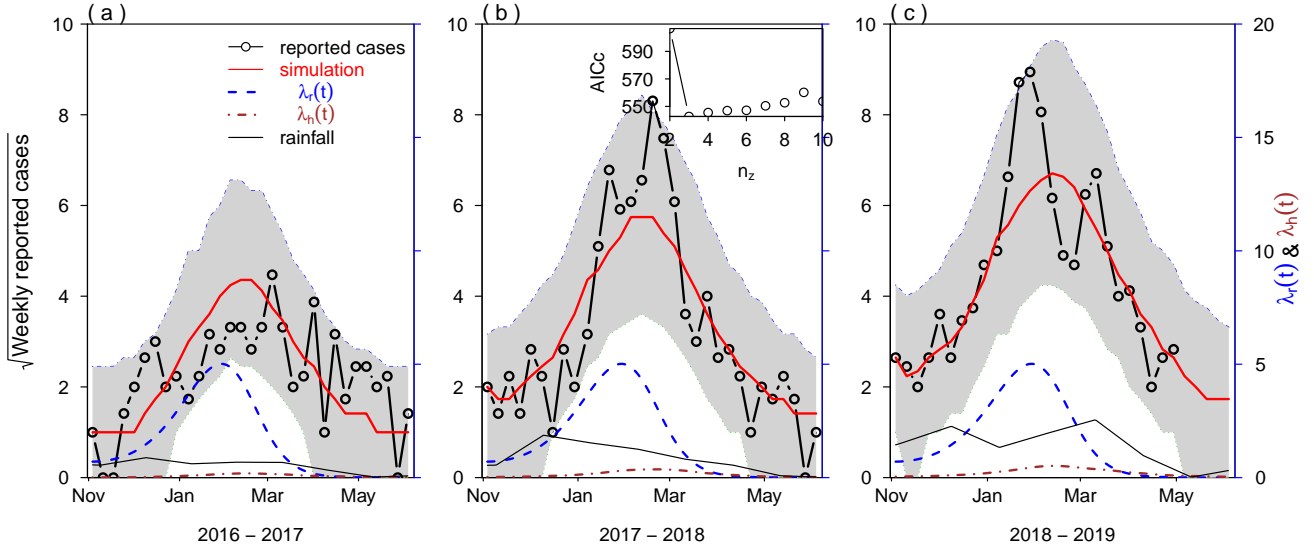
9

Figure 3: Fitting forces of infection of the model (2.1) by using the cubic spline function for scheme II. The black circles are the observed numbers of LHF cases, and the red solid lines are the simulation medians. The grey shaded regions represent the 95% CIs from the simulation. The black curve (thick line) represents the rainfall with delay of 145 days. The blue dashed line represents the force of infection from rodents, λ_r; and the brown dot-dashed line represents the force of infection from humans, λ_h. The parameter estimates are summarized in Table 3. The inset panel in (b) shows the AICc as a function of n_z, the number of nodes in the cubic spline. Since $n_z = 3$ attains the minimum AICc, thus $n_z = 3$ was used in (a-c).

years. If we denote the FoI as $\lambda = \beta I_r$, the case prevalence rate should be $\lambda S_h \propto \mathcal{R}_{\text{eff}} I_r$. Therefore, the estimated increase in the $s_h(0)$ across years could be due to an increase in the transmissibility (β), and amount of infected rodents (I_r). Since $\lambda S_h \propto \mathcal{R}_{\text{eff}} I_r = \mathcal{R}_0 S_h I_r$, the transmissibility and susceptibility cannot be disentangled.

In scheme I, the assumption $\beta_4 = \beta_8$ does not improve the fitting result extensively. We also show that β_5 ($\beta_5 = \beta_6 = \beta_7$) is small, and β_1 ($\beta_1 = \beta_2 = \beta_3$) is relatively high, this means that human-to-human transmission is relatively high (or comparable to rodent-to-human and rodent-to-rodent transmission, respectively), where the human-to-rodent transmission is negligible. In scheme II, we found that the maximum level, $\max\{\beta_4 I_r\} = \exp(7.248) \approx 1405.6$. However, at the steady state $I_r = N_r(1 - \frac{1}{\mathcal{R}_{0r}})$. The $\mathcal{R}_{0r}$ is the rodent only basic reproduction number (without human cases, i.e., the number of secondary infections that one infected rodent would reproduce if it is placed into a completely susceptible rodent population). Thus find the relationship between β_4 and $\mathcal{R}_{0r}$. Hence, $\max\{\beta_4 N_r(1 - \frac{1}{\mathcal{R}_{0r}})\} \approx 1405.6$. Note that, the $\frac{I_r}{N_r}$ is relatively high if $\mathcal{R}_{0r}$ is high. Therefore, we cannot extricate I_r and β_4, but we can find their relations.

4 Discussion

The transmission dynamics of LHF are mostly driven by zoonotic transmission involving human and rodent populations. The Lassa virus infections may spillover from rodent to human by

different transmission routes. Secondary infection between individuals may occur in large gatherings while individuals who develop clinical symptoms may seed the infection into hospital and generate nosocomial outbreaks [45]. The force of infection of LHF is largely influenced by seasonal and climatic factors that contribute eminently in the emergence of human cases. Attack rates appear to be lower in children than in adults [45]. The infection of LHF in rodent population appears to be asymptomatic (i.e., infectious but do not show symptoms) and temporary (after the infection the LHF virus can be cleared from the blood of an infected animal). However, the virus can be present in the urine of a rodent for more than 100 days. Further, both horizontal and vertical transmissions are possible for the LHF transmission [3]. Rodent to human transmission route has been considered as the major transmission path of the LHF infection, this is because the reservoir of the LHF is omnipresent per domestic rat; rodents are infected with the LHF virus in-utero and would stay infectious with the virus throughout its lifetime, excreting about 1,000 to 10,000 viral particles per milliliter of urine; the prevalence of the LHF in human and rodent is significantly influenced by the geographical correlations between them.

Mastomys natalensis rodents appear to be numerous in the forest resulting in high prevalence of the LHF in human population in forest area, while the proportion of the LHF infected rodents is higher in communities resulting in high infection rates in human population [3, 39]. Evidence shows that rodent consumers have a higher risk of LHF infection (which is about twice) than non-consumers, even though the association does not fulfill the conventional 5% significance threshold (with *p*-value of 0.10) [39]. We used a mechanistic modelling technique and data fitting to explore the transmission dynamics of the annual LHF epidemics in Nigeria from 2016-2019. The findings in this work provide a better understanding of the patterns and driving forces of the LHF outbreaks in endemic areas, which is to the best of our knowledge was not reported in the prior studies. The iterated filtering statistical inference framework was used on the model (2.1) for the data fitting. The model (2.1) was fitted to time series data on LHF cases in Nigeria from 2016-19 in Fig 2 and 3 using two different schemes. The proposed LHF epidemic model was able to predict the LHF epidemics in Nigeria from 2016-19 under biologically reasonable settings.

In Fig. 2, we reveal the dynamics of the rodent population by incorporating a time-dependent rodent population size even though the information on LHF prevalence among rodent is inadequate. Thus, the model fitting result suggests that the observed human outbreaks are a combination effect of the rodent outbreaks together with time-dependent (basically a step-function type) of transmission rate from rodent to human (or spill-over rate). The result also highlights the existence of LHF outbreaks among rodents in the first half of each year. The parameter $\beta_4(t)$ takes the maximum value between Nov and Feb of every year, after which the value drops to a minimum. Our fitting result gives one possible scenario which can explain the annual outbreaks of LHF. The increasing amplitude of LHF could be explained by higher initial infectious human cases in Nov 2017 and 2018 than in Nov 2016. We assumed the transmission rates to be identical across the three years outbreaks. The higher initial infectious human cases could be due to higher rainfall in 2017 and 2018 than in 2016, even though there could be other possible scenarios. However, more knowledge on the rodent population (population size and virus prevalence) could be helpful to figure out the true scenario. Nevertheless, this work is the first attempt to analyze these outbreak data through mechanistic modeling framework.

We found that the epidemics in each year could be reconstructed by the same FoI's (i.e., $\lambda_h(t)$), and also could be estimated with the same model structure. The similarity of patterns in the data leads to a presumption that the driving force (from rodent) of the epidemic could have the same or similar pattern across years, or could be completely be periodic or may differ only by a factor.

11

The proposed reconstruction approach presents equivalent goodness-of-fit in terms of the values of log-likelihood. In Fig. 3 we assumed that all human cases were explained as rodent infected, since the $\beta_4(\mu_v(t))$ is much larger than β_1. And the observed outbreak among human were explained by either an outbreak among rodent (if the spill-over rate is constant) or the time-varying spill-over and a constant prevalence of the LHF among rodent, or a combination of these both effects. We ignored the detailed dynamics of rodent, and simply modeled the transmission rate from rodent as time dependent. The reason to choose this scheme is for lack information on rodent (such as population size and LHF prevalence among rodent).

We also explored the sub-exponential growth feature in the LHF epidemics. Fig A3 is the fitting results of the weekly reported cases of the LHF using the sub-exponential growth formulation adopted from [13, 14], which highlights the positive impact in obtaining the accurate assessment of the effective reproduction number of the LHF outbreaks.

The model parameters and reconstructed rodent infections set a reasonable modeling framework for further improvement. The model also allows simulation-based analysis to evaluate the practical control measures. The initial susceptibility ($S_h(t)$) is increased from 2016 to 2017 and from 2017 to 2018, by a factor of (roughly) 2 each year. However, this could be due to the assumption that the rates of transmission of the three years were identical (including both human-to-human, and rodent-to-human transmissions). Given that the initial susceptibility and transmission rates cannot be disentangled in reality, it could be that the initial susceptibility had been kept the same at the beginning of the three years, then the transmission rates had been increased by a factor of 2 from year to year. Nevertheless, the transmission rate shared strikingly similar temporal patterns, as this can be seen from the raw data.

Although our basic model contained both human and rodent populations, the fitting result was able to capture dynamical features of the human population and some of the rodent population. We presumed that it could be sufficient to synthesize all rodent-contributed infections (to human) as one time-dependent function in the analysis. Furthermore, our model could also be extended to incorporate weather and climate data into the rodent contributed infections. This is to replace the flexible cubic spline with a mechanistic form which could give more detailed dynamics features of the LHF epidemics.

We reveal that the estimated FoI's exhibited similar seasonal patterns from 2016-2019, however, not all of them were synchronized in each year despite their proximity. These results also can be extended on the LHF transmissibility in terms of the effective reproduction number. We also allowed the initial condition of the susceptibility to vary across years and to be estimated between 0 and 1. Although we have restricted the major FoI (rodent ro human) to be the same across years for the fitting simplicity, it is more likely to be variable in practice. Thus, the estimated increase in the initial susceptibility actually reflects an increase in the case prevalence rate across years. Therefore, the estimated increase in the initial susceptibility across years could be due to the increase in the transmissibility (in terms of effective transmission rate, β), or amount of infected rodents (reflected by the number of infected cases, I_r), or joint effect of β and I_r (e.g., in terms of FoI, $\lambda = \beta I_r$) in each year.

Our model was able to capture numerous dynamical features, even though some features were missed due to the insufficiency of the data, especially in the rodent population. This part is left for future analysis when the data becomes available. Further analysis and numerical results show that our model exhibits forward bifurcation (exchanges of stability between the disease-free equilibrium and the endemic equilibrium when the basic reproduction number equals one, see Appendix A1 for detail). The sensitivity analysis in Appendix A2 also reveals the top-ranked parameters (i.e., rodent-

to-human transmission rate, the maximum growth rate of the rodents, and the rodent mortality) that could be important for the LHF control.

Table 3: Baseline values and ranges for parameters of model (2.1).

Parameter	Baseline (Range)	Units	Sources	Fitting status
N_h	5×10^7 (2 - 10×10^7)	Persons	Estimated by [65]	Fixed
μ_h	0.00005 (0.00003 - 0.00006)	Day^{-1}	Estimated by [53]	Fixed
μ_r	0.002 (0.001 - 0.006)	Day^{-1}	[61]	Fixed
Π_h	2500 (1000 - 5000)	Persons day^{-1}	Estimated by [65]	Fixed
K	4000 (2000 - 10000)	Rodents	Assumed	Fixed
σ_1	0.52 (0.1 - 1)	Day^{-1}	Estimated by [1]	Fixed
σ_2	0.41 (0.1 - 1)	Day^{-1}	Estimated by [1]	Fixed
α_1	0.0123 (0.001 - 0.025)	Day^{-1}	Estimated by [2]	Fixed
α_2	0.012 (0.0015 - 0.025)	Day^{-1}	Estimated by [2]	Fixed
γ	0.1 (0.09 - 0.51)	Day^{-1}	Estimated by [60]	Fixed
ξ	0.0067 (0.0035 - 0.03)	Day^{-1}	Estimated by [60]	Fixed
$\tau_1 = \tau_2 = \tau_3$	0.0517 (0 - 1)	Day^{-1}	Assumed	Fixed
δ_1	0.21 (0.1 - 0.5)	Day^{-1}	[51]	Fixed
δ_2	0.2 (0.1 - 0.5)	Day^{-1}	[51]	Fixed
δ_3	0.19 (0.1 - 0.5)	Day^{-1}	[51]	Fixed
b	41 (35 - 50)	Day^{-1}	Assumed	Fixed
$\beta_1 = \beta_2 = \beta_3$	0.22 (0.03 - 0.5)	Day^{-1}	Estimated by [18]	Fixed, to be estimated
β_4	0.3045 (0.1 - 0.8)	Day^{-1}	[1]	Time-varying, to be estimated
$\beta_5 = \beta_6 = \beta_7$	0.075 (0.03 - 0.2)	Day^{-1}	Assumed	Fixed, to be estimated
β_8	0.142 (0.05 - 0.4)	Day^{-1}	Assumed	Time-varying, to be estimated

Declarations

Ethics approval and consent to participate   Since no personal data was collected, the ethical approval or individual consent was not applicable.

Availability of data and materials   The Lassa fever cases surveillance data used in this work were freely obtained via the public domains [50]. The data may also be available based on request.

Funding   This work was not funded.

Acknowledgements   The authors are grateful to the editor and anonymous reviewers for their perceptive and positive comments.

Disclaimer   The funding agencies had no role in the design and conduct of the study; collection, management, analysis, and interpretation of the data; preparation, review, or approval of the manuscript; or decision to submit the manuscript for publication.

Conflict of Interests   The authors declared that they have no competing interests.

Authors' Contributions   SSM and DH conceived the study, and drafted the first manuscript. SSM, SZ, QL and DH carried out the study. CG and GD critically revised the manuscript. All authors gave final approval for publication.

References

[1] F. B. Agusto, Mathematical model of Ebola transmission dynamics with relapse and reinfection, *Math. Biosci.*, **283** (2017), 48-59, http://dx.doi.org/10.1016/j.mbs.2016.11.002.

[2] F. B. Agusto, M. I. Teboh-Ewungkem and A. B. Gumel, Mathematical assessment of the effect of traditional beliefs and customs on the transmission dynamics of the 2014 Ebola outbreaks, *BMC Med.*, **13** (2015), 96, https://doi.org/10.1186/s12916-015-0318-3.

[3] A. R. Akhmetzhanov, Y. Asai and H. Nishiura, Quantifying the seasonal drivers of transmission for Lassa fever in Nigeria, *Phil. Trans. R. Soc. -B*, **374** (2019), 20180268. http://dx.doi.org/10.1098/rstb.2018.0268.

[4] O. C. Akhuemokhan, R. O. Ewah-Odiase, N. Akpede, et al., Prevalence of Lassa virus disease (LVD) in Nigerian children with fever or fever and convulsions in an endemic area, *PLoS Negl. Trop. Dis.*, **11** (2017), e0005711, https://doi.org/10.1371/journal.pntd.0005711.

[5] K. G. Andersen, J. B. Shapiro, C. B. Matranga, et al., Clinical sequencing uncovers origins and evolution of Lassa virus, *Cell*, **162** (2015), 738-750, http://dx.doi.org/10.1016/j.cell.2015.07.020.

[6] M. D. Bajanil, O. Tomo, P. E. Rollin, et al., A survey for antibodies to Lassa virus among health workers in Nigeria, *Trans. R. Soc. Trop. Med. Hyg.*, **91** (1997), 379-381, https://doi.org/10.1016/S0035-9203(97)90247-9.

[7] C. Breto, D. He, E. L. Ionides, et al, Time series analysis via mechanistic models, *Ann. Appl. Stat.*, **3** (2009), 319-348, http://dx.doi.org/10.1214/08-AOAS201.

[8] G. S. Bowen, O. Tomori, H. Wulff, et al., Lassa fever in Onitsha, East Central State, Nigeria, in 1974, *Bull. World Health Org.*, **52** (1975), 599-604.

[9] A. Camacho, S. Ballesteros, A. L. Graham, et al., Explaining rapid reinfections in multiple-wave influenza outbreaks: Tristan da Cunha 1971 epidemic as a case study, *Proc. Biol. Sci.*, **278** (2011), 3635-43, pmid:21525058, https://doi.org/10.1098/rspb.2011.0300.

[10] D. E. Carey, G. E. Kemp, H. A. White, et al., Lassa fever epidemiological aspects of the 1970 epidemic, Jos, Nigeria, *Trans. R. Soc. Trop. Med. Hyg.*, **66** (1972), 402-408, https://doi.org/10.1016/0035-9203(72)90271-4.

[11] J. Carr, *Applications of centre manifold theory*, Springer, New York, 1981.

[12] C. Castillo-Chavez and B. Song, Dynamical model of tuberculosis and their applications, *Math. Biosci. Eng.*, **1** (2004), 361-404.

[13] G. Chowell, L. Sattenspiel, S. Bansal and C. Viboud, Mathematical models to characterize early epidemic growth: A review, *Phy. Life Rev.*, **18** (2016), 66-97. https://doi.org/10.1016/j.plrev.2016.07.005.

[14] G. Chowell, C. Viboud, L. Simonsen, S. M. Moghadas, Characterizing the reproduction number of epidemics with early subexponential growth dynamics, *J. R. Soc. Interface*, **13** (2016), 0659. http://dx.doi.org/10.1098/rsif.2016.0659.

[15] C. G. Coetzee, The breeding season of the multimammate mouse *Praomys (Mastomys) Natalensis* (A. Smith) in the Transvaal highveld, *Zoolog. Afric.*, **1** (1965), 29-39. DOI:10.1080/00445096.1965.11447297.

[16] A. H. Demby, A. Inapogui, K. Kargbo, J. Koninga, K. Kourouma, *et al.*, Lassa Fever in Guinea: II. Distribution and Prevalence of Lassa Virus Infection in Small Mammals, *Vector Borne Zoonotic Dis.*, **4** (2004). https://doi.org/10.1089/15303660160025912.

[17] R. Bürger, G. Chowell, E. Gavilán, P. Mulet, L. M. Villada. Numerical solution of a spatio-temporal predator-prey model with infected prey, *Math. Biosci. Eng.*, 16(1) (2019), 438-473. https://doi.org/10.3934/mbe.2019021.

[18] A. Dénes and A. B. Gumel, Modelling the impact of quarantine during an outbreaks of Ebola virus disease, *Infect. Dis. Model.*, **4** (2019), 12-27, https://doi.org/10.1016/j.idm.2019.01.003.

15

[19] O. Diekmann, J. Heesterbeek and J. Metz, On the definition and the computation of the basic reproduction ratio R_0 in models for infectious diseases in heterogeneous populations, *J. Math. Biol.*, **28** (1990), 365-382, https://doi.org/10.1007/BF00178324.

[20] D. J. Earn, D. He, M. B. Loeb, et al., Effects of school closure on incidence of pandemic influenza in Alberta, Canada, *Ann. Intern. Med.*, **156** (2012), 173-181, http://annals.org/aim/article-abstract/1033342.

[21] E. Fichet-Calvet, B. Becker-Ziaja, L. Koivogui, et al., Lassa serology in natural populations of rodents and horizontal transmission, *Vector Bone Zoonotic Dis.*, **14** (2014), https://doi.org/10.1089/vbz.2013.1484.

[22] E. Fichet-Calvet, E. Lecompte, L. Koivogui, *et al.*, Fluctuation of abundance and Lassa virus prevalence in mastomys natalensis in Guinea, west Africa, *Vector Borne Zoonotic Dis.*, **7** (2007), 119-128, https://doi.org/10.1089/vbz.2006.0520.

[23] E. Fichet-Calvet and D. J. Rogers, Risk Maps of Lassa fever in west Africa, *PLoS Negl. Trop. Dis.*, **3** (2009), e388, https://doi.org/10.1371/journal.pntd.0000388.

[24] S. P. Fisher-Hoch, O. Tomori, A. Nasidi, et al., Review of cases of nosocomial Lassa fever in Nigeria: the high price of poor medical practice, *Brit. Med. J.*, **311** (1995), 857, https://doi.org/10.1136/bmj.311.7009.857.

[25] F. Forouzannia and A. B. Gumel, Mathematical analysis of an age-structured model for malaria transmission dynamics, *Math. Biosci.*, **247** (2014), 80-94, https://doi.org/10.1016/j.mbs.2013.10.011.

[26] S. M. Garba, A. B. Gumel and M. R. A. Bukar, Backward bifurcations in dengue transmission dynamics, *Math. Biosci.*, **215** (2008), 11-25, https://doi.org/10.1016/j.mbs.2008.05.002.

[27] D. Gao, Y. Lou Y, D. He, et al., Prevention and control of zika as a mosquito-borne and sexually transmitted disease: a mathematical modelling analysis, *Sci. Rep.*, **6** (2016), 28070, https://doi.org/10.1038/srep28070 PMID: 27312324.

[28] E. L. Hamblion, P. Raftery, A. Wendland, et al., The challenges of detecting and responding to a Lassa fever outbreak in an Ebola-affected setting, *Int. J. Infect. Dis.*, **66** (2018), 65-73, https://doi.org/10.1016/j.ijid.2017.11.007.

[29] D. He, J. Dushoff, T. Day, J. L. Ma, D. J. D. Earn, Mechanistic modelling of the three waves of the 1918 influenza pandemic, *Theory Ecol.*, **4** (2011), 283-8, https://doi.org/10.1007/s12080-011-0123-3.

[30] D. He, D. Gao, Y. Lou Y, *et al.*, A comparison study of zika virus outbreaks in French Polynesia, Colombia and the State of Bahia in Brazil, *Sci. Rep.*, **7** (2017), 273, https://doi.org/10.1038/s41598-017-00253-1.

[31] D. He, E. L. Ionides and A. A. King, Plug-and-play inference for disease dynamics: measles in large and small populations as a case study, *J. R. Soc. Interf.*, **7** (2010), 271-283, https://doi.org/10.1098/rsif.2009.0151.

[32] D. He, R. Lui, L. Wang, *et al.*, Global spatio-temporal patterns of influenza in the post-pandemic era, *Sci. Rep.*, **5** (2015), 11013, http://doi:10.1038/srep11013.

[33] N. Hussaini, J. M-S. Lubuma, K. Barley, et al., Mathematical analysis of a model for AVL - HIV co-endemicity, *Math. Biosci.*, **271** (2016), 80-95, https://doi.org/10.1016/j.mbs.2015.10.008.

[34] E. L. Ionides, A. Bhadra, Y. Atchade, et al., Iterated filtering, *Ann. Stat.*, **39** (2011), 1776-1802, http://dx.doi.org/10.1214/11-AOS886.

[35] E. L. Ionides, C. Breto and A. A. King, Inference for nonlinear dynamical systems, *Proc. Natl. Acad. Sci.*, **103** (2006), 18438-18443, https://doi.org/10.1073/pnas.0603181103.

[36] G. L. Iacono, A. A. Cunningham, E. Fichet-Calvet, et al., Using modelling to disentangle the relative contributions of zoonotic and anthroponotic transmission: the case of Lassa fever, *PLOS Negl. Trop. Dis.*, **9** (2015), e3398, https://doi.org/10.1371/journal.pntd.0003398.

[37] T. O. James, S. T. Akinyemi and B. Oluwade, Stability analysis of Lassa fever with quarantine and permanent immunity, *Int. J. Appl. Sci. Math. Theory.*, **1** (2015), 71-81.

[38] D. F. John, B. J. Peter, E. Y. Jacob, et al., Endemic Lassa fever in Liberia. II. serological and virological findings in hospital patients, *Trans. R. Soc. Trop. Med. Hyg.*, **78** (1984), 656-660, https://doi.org/10.1016/0035-9203(84)90232-3.

[39] S. Kerne'is, L. Koivogui, N. Magassouba, K. Koulemou, R. Lewis, *et al.*, Prevalence and risk factors of Lassa seropositivity in inhabitants of the forest region of Guinea: a cross-sectional study, *PLoS Negl. Trop. Dis.*, **3** 11 (2009), e548. doi:10.1371/journal.pntd.0000548.

[40] S. H. Khan, A. Goba, M. Chu, et al., New opportunities for field research on the pathogenesis and treatment of Lassa fever, *Antiv. Research*, **78** (2008), 103-115, https://doi.org/10.1016/j.antiviral.2007.11.003.

[41] A. A. King, D. Nguyen and E. Ionides, Statistical inference for partially observed Markov processes via the R package pomp, *J. Stat. Softw.*, **69** (2016), 1-43.

[42] Q. Lin, Z. Lin, A. P. Y. Chiu, et al., Seasonality of influenza A(H7N9) virus in China -fitting simple epidemic models to human cases, *PLoS One*, **11** (2016), e0151333, https://doi.org/10.1371/journal.pone.0151333.

[43] J. B. McCormick, P. A. Webb, J. W. Krebs, K. M. Johnson and E. S. Smith, A prospective study of the epidemiology and ecology of Lassa fever, *J. Infect. Dis.*, **155** (1987), 437-444, https://doi.org/10.1093/infdis/155.3.437.

[44] J. T. Meulen, M. Badusche, K. Kuhnt, A. Doetze, J. Satoguina, *et al.*, Characterization of human CD4+ T-cell clones recognizing conserved and variable epitopes of the Lassa virus nucleoprotein, *J. Virol.*, **74** (2000), 2186-2192, https://doi.org/10.1128/JVI.74.5.2186-2192.2000

[45] T. P. Monath, Lassa fever: review of epidemiology and epizootiology, *Bull. World Health Organ.*, **52** (1975), 577-592.

[46] T. P. Monath, V. F. Newhouse, G. E. Kemp, H. W. Setzer and A. Cacciapuoti, Lassa virus isolation from Mastomys natalensis rodents during an epidemic in Sierra Leone, *Science*, **185** (1974), 263-265.

[47] S. S. Musa, S. Zhao, H. S. chan, Z. Jin and D. He, A mathematical model to study the 2014-2015 large-scale dengue epidemics in Kaohsiung and Tainan cities in Taiwan, China, *Math. Biosci. Eng.*, **16** (2019), 3841-3863, http://dx.doi.org/10.3934/mbe.2019190.

[48] S. S. Musa, S. Zhao, N. Hussaini, A. G. Habib and D. He, Mathematical modeling and analysis of Meningococcal Meningitis transmission dynamics, *Int. J. Biomath.*, (2019), https://doi.org/10.1142/S1793524520500060.

[49] S. S. Musa, N. Hussaini, S. Zhao, D. He, Dynamical analysis of chikungunya and dengue co-infection model, *Disc. Cont. Dyn. Syst. - B*, **22** (2019), 1-27. https://doi.org/10.3934/dcdsb.2020009.

[50] Nigeria Centre for Disease Control, Disease situation report: an update of Lassa fever outbreak in Nigeria, 2019. Available from: https://www.ncdc.gov.ng/ and https://www.ncdc.gov.ng/diseases/sitreps.

[51] O. S. Obabiyi and A. A. Onifade, Mathematical model for Lassa fever transmission dynamics with variable human and reservoir population, *Int. J. Diff. Eqn. Appl.*, **1** (2017), 67-91.

[52] P. Okokhere, A. Colubri, C. Azubike, et al., Clinical and laboratory predictors of Lassa fever outcome in a dedicated treatment facility in Nigeria: a retrospective, observational cohort study, *Lancet Infect. Dis.*, **18** (2018), 684-695, https://doi.org/10.1016/S1473-3099(18)30121-X.

[53] K. Okuneye and A. B. Gumel, Analysis of a temperature- and rainfall-dependent model for malaria transmission dynamics, *Math. Biosci.*, **287** (2017), 72-92, https://doi.org/10.1016/j.mbs.2016.03.013.

[54] M. O. Onuorah, N. I. Akinwande, M. O. Nasir, et al., Sensitivity analysis of Lassa fever model, *Int. J. Math. Stat. Std.*, **4** (2016), 30-49.

[55] J. K. Richmond and D. J. Baglole, Lassa fever: epidemiology, clinical features, and social consequences, *Bri. Med. J.*, **327** (2003), 1271, https://doi.org/10.1136/bmj.327.7426.1271.

17

[56] C. R. Rocha, R. Ribeiro and J. Marinho-Filho, Influence of temporal variation and seasonality on population dynamics of three sympatric rodents, *Mammalian Biol.*, **84** (2017), 20-29, https://doi.org/10.1016/j.mambio.2017.01.001.

[57] P. Roop-O, W. Chinviriya and S.Chinviriyasit, The effect of incidence function in backward bifurcation for malaria model with temporary immunity, *Math. Biosci.*, **265** (2015), 47-64, https://doi.org/10.1016/j.mbs.2015.04.008.

[58] A. M. Saez, M. C. Haidara, A. Camara, F. Kourouma, M. Sage, N. Magassouba, *et al.*, Rodent control to fight Lassa fever: evaluation and lessons learned from a 4-year study in Upper Guinea, *PLoS Negl. Trop. Dis.*, **12** (2018), e0006829. https://doi.org/10.1371/journal.pntd.0006829.

[59] M. A. Safi and A. B. Gumel, Dynamics of a model with quarantine-adjusted incidence and quarantine of susceptible individuals, *J. Math. Anal. Appl.*, **399** (2013), 565-575, https://doi.org/10.1016/j.jmaa.2012.10.015.

[60] M. A. Safi and A. B. Gumel, Qualitative study of a quarantine/isolation model with multiple disease stages, *Appl. Math. Comput.*, **218** (2011), 1941-1961, https://doi.org/10.1016/j.amc.2011.07.007.

[61] P. Sengupta, The laboratory rat: relating its age with humans, *Int. J. Prev. Med.*, **4** (2013), 624-630.

[62] C. P. Simon and J. A. Jacquez, Reproduction numbers and the stability of equilibrium of SI models for heterogeneous populations, *SIAM J. Appl. Math.*, **52** (1992), 541-576, https://doi.org/10.1137/0152030.

[63] J. Ter Meulen, I. Lukashevich, K. Sidibe, A. Inapogui, M. Marx, *et al.*, Hunting of Peridomestic Rodents and Consumption of Their Meat as Possible Risk Factors for Rodent-to-Human Transmission of Lassa Virus in the Republic of Guinea, *Amer. J. Trop. Med. Hyg.*, **55** 6 (1996), 661-666. https://doi.org/10.4269/ajtmh.1996.55.661.

[64] The website of R package POMP: statistical inference for partially-observed Markov processes, 2018. Available from: https://kingaa.github.io/pomp/.

[65] The World Bank demography. Nigeria, 2019. Available from: https://data.worldbank.org/country/nigeria.

[66] S. Usaini, U. T. Mustapha and S. S. Musa, Modelling scholastic underachievement as a contagious disease, *Math. Meth. Appl. Sci.*, **41** (2018), 8603-8612, https://doi.org/10.1002/mma.4924.

[67] P. van den Driessche and J. Watmough, Reproduction numbers and sub-threshold endemic equilibria for compartmental models of disease transmission, *Math. Biosci.*, **180** (2002), 29-48, https://doi.org/10.1016/S0025-5564(02)00108-6.

[68] World Heath Organization, Lassa fever, 2018. Available from: http://www.who.int/news-room/fact-sheets/detail/lassa-fever.

[69] S. Xiao, H. Zhang, Y. Yang, et al., Partial virus (arenaviradae) infection in the Syrian golden hamster, mesocricetus auratus: a new animal model for arenaviral hemorrhagic fever, *Am. J. Trop. Med. Hyg.*, **64** (2001), 111-118, https://doi.org/10.4269/ajtmh.2001.64.111.

[70] S. Zhao, S. S. Musa, H. Fu, D. He, J. Qin, Large-scale Lassa fever outbreaks in Nigeria: quantifying the association between disease reproduction number and local rainfall, *Epidemiol. Infect.*, **148** (2020), 1-12, https://doi.org/10.1017/S0950268819002267.

[71] S. Zhao, S. S. Musa, H. Fu, D. He, J. Qin, Simple framework for real-time forecast in a data-limited situation: the Zika virus (ZIKV) outbreaks in Brazil from 2015 to 2016 as an example. Parasites & vectors, **12** (2019), 344, https://doi.org/10.1186/s13071-019-3602-9.

[72] S. Zhao, Y. Lou, A. P. Chiu, et al., Modelling the skip-and-resurgence of Japanese encephalitis epidemics in Hong Kong, *J. Theor. Biol.*, **454** (2018), 1-10, https://doi.org/10.1016/j.jtbi.2018.05.017.

[73] S. Zhao, L. Stone, D. Gao, et al., Modelling the large-scale yellow fever outbreak in Luanda, Angola, and the impact of vaccination, *PLoS Negl. Trop. Dis.*, **12** (2018), e0006158, https://doi.org/10.1371/journal.pntd.0006158.

Appendices

A1 Mathematical analysis

A1.1 Disease-free equilibrium and basic reproduction number

The model (2.1) will be analyzed to gain insight into its dynamical features. The total human and rodent populations satisfy the following equations

$$\frac{dN_h(t)}{dt} = \Pi_h - \mu_h N_h - \delta_1 I_h - \delta_2 I_q - \delta_3 H \leq \Pi_h - \mu_h N_h,$$

and

$$\frac{dN_r(t)}{dt} = b\left(1 - \frac{N_r}{K}\right)N_r - \mu_r(S_r + I_r) = N_r\left(b - \mu_r - \frac{b}{K}N_r\right).$$

Denote $\Omega = \left\{(S_h, E_h, I_h, E_q, I_q, H, R, S_r, I_r) \in \mathbb{R}_+^9 : N_h \leq \frac{\Pi_h}{\mu_h} : N_r \leq \frac{K(b-\mu_r)}{b}\right\}$. It can be shown (by solving N_h and N_r) that all solutions of the system starting in the region Ω remain in Ω for all $t > 0$. Thus, the region Ω is positively invariant, and it is sufficient to consider solutions in Ω. In this region, the usual existence, uniqueness and continuity results hold for the system [25, 33, 66, 48, 49].

The model (2.1) has a unique disease-free equilibrium (DFE), obtained by setting the right-hand sides of the model equations to zero, given by

$$E_0 = (S_h^0, E_h^0, I_h^0, E_q^0, I_q^0, H^0, R^0, S_r^0, I_r^0) = \left(\frac{\Pi_h}{\mu_h}, 0, 0, 0, 0, 0, 0, \frac{K(b - \mu_r)}{b}, 0\right).$$

The matrices F (for the new infection terms) and V (for the transition terms) associated with the model (2.1) are given, respectively, by

$$F = \begin{bmatrix} 0 & C_1 & 0 & C_2 & C_3 & C_4 \\ 0 & 0 & 0 & 0 & 0 & 0 \\ 0 & 0 & 0 & 0 & 0 & 0 \\ 0 & 0 & 0 & 0 & 0 & 0 \\ 0 & 0 & 0 & 0 & 0 & 0 \\ 0 & C_5 & 0 & C_6 & C_7 & C_8 \end{bmatrix} \text{ and } V = \begin{bmatrix} Q_1 & 0 & 0 & 0 & 0 & 0 \\ -\sigma_1 & Q_2 & 0 & 0 & 0 & 0 \\ -\gamma & 0 & Q_3 & 0 & 0 & 0 \\ 0 & 0 & -\sigma_2 & Q_4 & 0 & 0 \\ 0 & -\alpha_1 & 0 & -\alpha_2 & Q_5 & 0 \\ 0 & 0 & 0 & 0 & 0 & \mu_r \end{bmatrix},$$

where,

$$Q_1 = \sigma_1 + \gamma + \mu_h, \quad Q_2 = \tau_1 + \alpha_1 + \delta_1 + \mu_h, \quad Q_3 = \sigma_2 + \mu_h, \quad Q_4 = \tau_2 + \alpha_2 + \delta_2 + \mu_h,$$

$$Q_5 = \tau_3 + \delta_3 + \mu_h, \quad Q_6 = \xi + \mu_h, \quad C_1 = \beta_1, \quad C_2 = \beta_2, \quad C_3 = \beta_3, \quad C_4 = \frac{\beta_4 \Pi_h}{\mu_h}$$

$$C_5 = \frac{\beta_5 K(b - \mu_r)}{b}, \quad C_6 = \frac{\beta_6 K(b - \mu_r)}{b}, \quad C_7 = \frac{\beta_7 K(b - \mu_r)}{b}, \quad \text{and} \quad C_8 = \beta_8.$$

Hence,

$$\mathcal{R}_0 = \rho(FV^{-1}) = \frac{g_1 + \sqrt{g_2}}{g_3}, \tag{A1-1}$$

where,

$$g_1 = (\gamma \sigma_2 (C_2 Q_5 + C_3 \alpha_2) Q_2 + Q_4 Q_3 \sigma_1 (C_1 Q_5 + C_3 \alpha_1)) \mu_r + C_8 Q_1 Q_2 Q_3 Q_4 Q_5,$$

$$g_2 = (\gamma \sigma_2 (C_2 Q_5 + C_3 \alpha_2) Q_2 + Q_4 Q_3 \sigma_1 (C_1 Q_5 + C_3 \alpha_1))^2 \mu_r{}^2 - C_8{}^2 Q_1{}^2 Q_2{}^2 Q_3{}^2 Q_4{}^2 Q_5{}^2 +$$
$$2 Q_4 Q_5 Q_1 Q_3 \cdot ((-2 C_6 C_4 + C_2 C_8) Q_5 + \alpha_2 (C_3 C_8 - 2 C_7 C_4)) \gamma \sigma_2 Q_2 + 2 Q_1 Q_3 Q_4^2 Q_5$$
$$((C_1 C_8 - 2 C_5 C_4) Q_5 + \alpha_1 (C_3 C_8 - 2 C_7 C_4)) \sigma_1 Q_3 Q_2 \mu_r,$$

$$g_3 = 2 Q_1 Q_2 Q_3 Q_4 Q_5 \mu_r.$$

Since we assume that, $\beta_1 = \beta_2 = \beta_3$ and $\beta_5 = \beta_6 = \beta_7$ so that $C_1 = C_2 = C_3$ and $C_5 = C_6 = C_7$. Using Theorem 2 of [67], the following result can be established.

Theorem A1.1. *The disease-free equilibrium, E_0, of the model* (2.1) *is locally asymptotically stable (LAS) if $\mathcal{R}_0 < 1$, and unstable if $\mathcal{R}_0 > 1$.*

The threshold quantity $\mathcal{R}_0$ represents the average number of secondary cases that one infectious individual would generate over the duration of the infectious period if introduced into a completely susceptible population [67, 71].

A1.2 Endemic equilibrium

The endemic equilibrium of the model (2.1) is the steady state where the disease persists in the population, that is, when at least one of the infected classes/compartments of the model is non-empty. Let $E^* = (S_h^*, E_h^*, I_h^*, E_q^*, I_q^*, H^*, R^*, S_r^*, I_r^*)$ be an endemic equilibrium solution of model (2.1). Then, equating the right hand side of Eqn (2.1) to zero, the endemic equilibrium in terms of the forces of

infection λ_h and λ_r, is given by,

$$S_h^* = \frac{Q_1 Q_2 Q_5 Q_6 \Pi_h Q_3 Q_4}{((U_1 - U_2) Q_2 - U_3) \lambda_h + U_4},$$

$$E_h^* = \frac{Q_2 Q_5 Q_6 \lambda_h \Pi_h Q_3 Q_4}{((U_1 - U_2) Q_2 - U_3) \lambda_h + U_4},$$

$$I_h^* = \frac{Q_5 Q_6 \lambda_h \Pi_h Q_3 Q_4 \sigma_1}{(U_5 - U_6) \lambda_h + U_4},$$

$$E_q^* = \frac{Q_4 Q_6 \lambda_h \gamma\, Q_2 Q_5 \Pi_h}{((U_1 - U_2) Q_2 - U_3) \lambda_h + U_4},$$

$$I_q^* = \frac{Q_6 \lambda_h \gamma\, Q_2 Q_5 \sigma_2 \Pi_h}{((U_1 - U_2) Q_2 - U_3) \lambda_h + U_4},$$

$$H^* = \frac{(\gamma\, Q_2 \alpha_2 \sigma_2 + Q_3 Q_4 \sigma_1 \alpha_1) Q_6 \lambda_h \Pi_h}{((U_1 - U_2) Q_2 - U_3) \lambda_h + U_4},$$

$$R_h^* = \frac{\lambda_h (U_7 + U_8) \Pi_h}{((U_1 - U_2) Q_2 - U_3) \lambda_h + U_4},$$

$$S_r^* = \frac{K \mu_r (b - \mu_r)}{b (\lambda_r + \mu_r)}, \quad \text{and} \quad I_r^* = \frac{\lambda_r K (b - \mu_r)}{b (\lambda_r + \mu_r)},$$

where

$U_1 = Q_1 Q_5 Q_6 Q_3 Q_4$, $U_2 = \xi\, \gamma\, \sigma_2 (\alpha_2 \tau_3 - Q_5 \tau_2)$, $U_3 = \xi\, Q_3 Q_4 \sigma_1 (\tau_1 Q_5 - \tau_3 \alpha_1)$,

$U_4 = Q_1 Q_2 Q_5 \mu_h Q_6 Q_3 Q_4$, $U_5 = Q_4 ((Q_1 Q_2 Q_6 - \xi\, \sigma_1 \tau_1) Q_5 - \xi\, \sigma_1 \tau_3 \alpha_1) Q_3$,

$U_6 = \xi\, \gamma\, Q_2 \sigma_2 (\alpha_2 \tau_3 - Q_5 \tau_2)$, $U_7 = \gamma\, \sigma_2 (\alpha_2 \tau_3 + Q_5 \tau_2) Q_2$, and $U_8 = Q_3 Q_4 \sigma_1 (\tau_1 Q_5 + \tau_3 \alpha_1)$.

A1.3 Bifurcation analysis

The bifurcation analysis is performed by using Center Manifold Theory as presented in Castillo-Chavez and Song [12]. Here, the conditions on the parameter values in the model (2.1) that cause forward or backward bifurcation to occur are analyzed [11, 12, 49, 67]. One can see that the backward bifurcation may not exist, which is probably due to the presence of the mass action incidence function in the model formulation, see for instance, [26, 57]. A forward bifurcation occurs when $\mathcal{R}_0$ crosses unity from below; a small positive asymptotically stable equilibrium appears and the disease-free equilibrium losses its stability [12].

Thus, forward bifurcation would occur at $\mathcal{R}_0 = 1$. This is illustrated by simulating the model (2.1) using the following parameter values, $\Pi_h = 11$, $\mu_h = 0.345 day^{-1}$, $\mu_r = 0.86 day^{-1}$, $K = 1500 day^{-1}$, $b = 625 day^{-1}$, $\sigma_1 = 0.85 day^{-1}$, $\sigma_2 = 0.80 day^{-1}$, $\alpha_1 = 0.23 day^{-1}$, $\alpha_2 = 0.23 day^{-1}$, $\gamma = 0.065 day^{-1}$, $\xi = 0.203 day^{-1}$, $\delta_1 = 0.21 day^{-1}$, $\delta_2 = 0.2 day^{-1}$, $\delta_3 = 0.19 day^{-1}$, $\tau_1 = 0.25 day^{-1}$, $\tau_2 = 0.27 day^{-1}$, $\tau_3 = 0.35 day^{-1}$, $\beta_1 = \beta_2 = ... = \beta_8 = 0.05 day^{-1}$; it should be stated that these parameter values are chosen for illustrative purpose only. With these set of parameters $\mathcal{R}_0 = 0.36337$, $A = -667.0934$ and $B = 0.8213$ (note that A and B are the associated bifurcation coefficients obtained) The forward bifurcation diagram of the model (2.1) is represented in Figure A1. Thus, the following result is established.
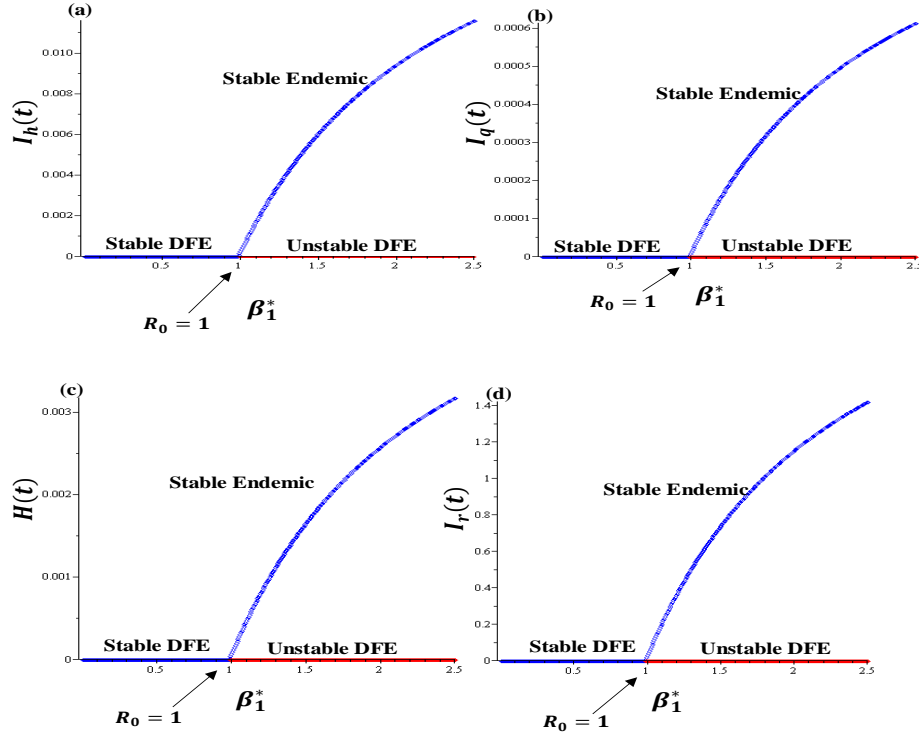
Figure A1: Forward bifurcation diagram of the model (2.1).

Theorem A1.2. *The LHF model* (2.1) *undergoes forward bifurcation at* $\mathcal{R}_0 = 1$ *whenever the bifurcation coefficients, A and B are negative and positive, respectively.*

Proof. The proof of the above theorem is based on the Centre Manifold Theory [11, 12, 49, 67]. Consider the system $\dfrac{dx}{dt} = f(x, \psi)$, where ψ is the bifurcation parameter, and f is continuously differentiable at least twice in both x and ψ. The disease-free equilibrium is the point $(x_0 = 0, \psi = 0)$ and the local stability of the disease-free equilibrium changes at the point $(x_0, 0)$ [67]. Now, we show that there is nontrivial equilibrium near the bifurcation point (x_0, ψ).

Suppose that $\beta_1 = \beta_1^*$ is chosen as a bifurcation parameter and we let $\mathcal{R}_0 = 1$ from Eqn (A1-1), then, by Theorem A1.1, the disease-free equilibrium, E_0, is locally stable when $\beta_1 < \beta_1^*$ and unstable when $\beta_1 > \beta_1^*$. Here $\beta_1 = \beta_1^*$ is a bifurcation value.

For convenience, let $S_h = x_1$, $E_h = x_2$, $I_h = x_3$, $E_q = x_4$, $I_q = x_5$, $H = x_6$, $R_h = x_7$, $S_r = x_8$, $I_r = x_9$, so that $N_h = x_1 + x_2 + x_3 + x_4 + x_5 + x_6 + x_7$ and $N_r = x_8 + x_9$. Further, by adopting the same vector notation with $x = (x_1, x_2, ..., x_9)^T$, the model (2.1) can be written as $\frac{dx}{dt} = f(x)$ where $f = (f_1, f_2, ..., f_9)^T$ is as follows:

$$f_1 = \Pi_h + \xi x_7 - \lambda_h x_1 - \mu_h x_1,$$
$$f_2 = \lambda_h x_1 - Q_1 x_2,$$
$$f_3 = \sigma_1 x_2 - Q_2 x_3,$$
$$f_4 = \gamma x_2 - Q_3 x_4,$$
$$f_5 = \sigma_2 x_4 - Q_4 x_5,$$
$$f_6 = \alpha_1 x_3 + \alpha_2 x_5 - Q_5 x_6, \tag{A2-1}$$
$$f_7 = \tau_1 x_3 + \tau_2 x_5 + \tau_3 x_6 - Q_6 x_7,$$
$$f_8 = b\left(1 - \frac{x_8 + x_9}{K}\right)(x_8 + x_9) - \lambda_r x_8 - \mu_r x_8,$$
$$f_9 = \lambda_r x_8 - \mu_r x_9,$$

where the associated forces of infection are respectively given by

$$\lambda_h = \frac{\beta_1 x_3 + \beta_2 x_5 + \beta_3 x_6}{\displaystyle\sum_{i=1}^{7} x_i} + \beta_4 x_9, \quad \text{and} \quad \lambda_r = \frac{\beta_8 x_9}{x_8 + x_9} + \beta_5 x_3 + \beta_6 x_5 + \beta_7 x_6. \tag{A2-2}$$

The Jacobian of the system (A2-1) , evaluated at the DFE (E_0) with $\beta_1 = \beta_1^*$, is given by

$$J(E_0) = F - V = \begin{bmatrix} -\mu_h & 0 & -\beta_1 & 0 & -\beta_2 & -\beta_3 & \xi & 0 & -n_1 \\ 0 & -Q_1 & \beta_1 & 0 & \beta_2 & \beta_3 & 0 & 0 & n_1 \\ 0 & \sigma_1 & -Q_2 & 0 & 0 & 0 & 0 & 0 & 0 \\ 0 & \gamma & 0 & -Q_3 & 0 & 0 & 0 & 0 & 0 \\ 0 & 0 & 0 & \sigma_2 & -Q_4 & 0 & 0 & 0 & 0 \\ 0 & 0 & \alpha_1 & 0 & \alpha_2 & -Q_5 & 0 & 0 & 0 \\ 0 & 0 & \tau_1 & 0 & \tau_2 & \tau_3 & -Q_6 & 0 & 0 \\ 0 & 0 & -n_2 & 0 & -n_3 & -n_4 & 0 & n_5 & n_6 \\ 0 & 0 & n_2 & 0 & n_3 & n_4 & 0 & 0 & n_7 \end{bmatrix}, \tag{A2-3}$$

where, $n_1 = \frac{\beta_4 \Pi_h}{\mu_h}$, $n_2 = \frac{\beta_5 K(b - \mu_r)}{b}$, $n_3 = \frac{\beta_6 K(b - \mu_r)}{b}$, $n_4 = \frac{\beta_7 K(b - \mu_r)}{b}$, $n_5 = -b + \mu_r$, $n_6 = -b + 2\mu_r - \beta_8$, $n_7 = \beta_8 - \mu_r$.

The Jacobian matrix $J(E_0)$ of the system (A2-1) has a simple zero eigenvalue (other eigenvalues have negative real parts). Hence, the CMT [12, 67] can be used to investigate the dynamics of the system (A2-1) located at $\beta_1 = \beta_1^*$ [12]. Using the notations in [12], the following computations are carried out.

Eigenvectors of $J(E_0)_{\beta_1 = \beta_1^*}$**:** For the case when $\mathcal{R}_0 = 1$ it can be shown that the $J(E_0)$ has a right eigenvector (corresponding to the zero eigenvalue), given by $\mathbf{w} = (w_1, w_2, ..., w_9)^T$, where

$$w_1 = \frac{-1}{\mu_h}\left(\frac{\beta_1\sigma_1}{Q_2} + \frac{\beta_2\sigma_2\gamma}{Q_3Q_4} + \frac{\beta_3}{Q_5}\left(\frac{\alpha_1\sigma_1}{Q_2} + \frac{\alpha_2\sigma_2\gamma}{Q_3Q_4}\right) - \frac{\xi}{Q_6}\left(\frac{\tau_1\sigma_1}{Q_2} + \frac{\tau_2\sigma_2\gamma}{Q_3Q_4} + \frac{\tau_3}{Q_5}\left(\frac{\alpha_1\sigma_1}{Q_2} + \frac{\alpha_2\sigma_2\gamma}{Q_3Q_4}\right)\right) - \right.$$

$$\left.\frac{n_1}{n_7}\left(\frac{n_2\sigma_1}{Q_2} + \frac{n_3\sigma_2\gamma}{Q_3Q_4} + \frac{n_4}{Q_5}\left(\frac{\alpha_1\sigma_1}{Q_2} + \frac{\alpha_2\sigma_2\gamma}{Q_3Q_4}\right)\right)\right)w_2,$$

$$w_2 > 0, \; w_3 = \frac{\sigma_1}{Q_2}w_2, \; w_4 = \frac{\gamma}{Q_3}w_2, \; w_5 = \frac{\sigma_2\gamma}{Q_3Q_4}w_2, \; w_6 = \frac{1}{Q_5}\left(\frac{\alpha_1\sigma_1}{Q_2} + \frac{\alpha_2\sigma_2\gamma}{Q_3Q_4}\right)w_2,$$

$$w_7 = \frac{1}{Q_6}\left(\frac{\tau_1\sigma_1}{Q_2} + \frac{\tau_2\sigma_2\gamma}{Q_3Q_4} + \frac{\tau_3}{Q_5}\left(\frac{\alpha_1\sigma_1}{Q_2} + \frac{\alpha_2\sigma_2\gamma}{Q_3Q_4}\right)\right)w_2,$$

$$w_8 = \frac{1}{n_5}\left(n_2\frac{\sigma_1}{Q_2} + n_3\frac{\sigma_2\gamma}{Q_3Q_4} + \frac{n_4}{Q_5}\left(\frac{\alpha_1\sigma_1}{Q_2} + \frac{\alpha_2\sigma_2\gamma}{Q_3Q_4}\right) + \frac{n_6}{n_7}\left(\frac{n_2\sigma_1}{Q_2} + \frac{n_3\sigma_2\gamma}{Q_3Q_4} + \frac{n_4}{Q_5}\left(\frac{\alpha_1\sigma_1}{Q_2} + \frac{\alpha_2\sigma_2\gamma}{Q_3Q_4}\right)\right)\right)w_2,$$

$$w_9 = \frac{-1}{n_7}\left(\frac{n_2\sigma_1}{Q_2} + \frac{n_3\sigma_2\gamma}{Q_3Q_4} + \frac{n_4}{Q_5}\left(\frac{\alpha_1\sigma_1}{Q_2} + \frac{\alpha_2\sigma_2\gamma}{Q_3Q_4}\right)\right)w_2.$$

Similarly, the components of the left eigenvector of $J(E_0)$ (corresponding to the zero eigenvalue), denoted by $\mathbf{v} = (v_1, v_2, ..., v_9)$, are given by

$$v_1 = 0, \; v_2 > 0, \; v_3 = \frac{1}{\sigma_1}\left(Q_1 - \frac{\gamma\sigma_2}{Q_3Q_4}\left(\beta_2 + \frac{\alpha_2}{Q_5}\left(\beta_3 - \frac{n_1n_4}{n_7}\right) - \frac{n_1n_3}{n_7}\right)\right)v_2,$$

$$v_4 = \frac{\sigma_2}{Q_3Q_4}\left(\beta_2 + \frac{\alpha_2}{Q_5}\left(\beta_3 - \frac{n_1n_4}{n_7}\right) - \frac{n_1n_3}{n_7}\right)v_2, \; v_5 = \frac{1}{Q_4}\left(\beta_2 + \frac{\alpha_2}{Q_5}\left(\beta_3 - \frac{n_1n_4}{n_7}\right) - \frac{n_3n_1}{n_7}\right)v_2,$$

$$v_6 = \frac{1}{Q_5}\left(\beta_3 - \frac{n_1n_4}{n_7}\right)v_2, \; v_7 = 0, \; v_8 = 0, \; v_9 = -\frac{n_1}{n_7}v_2.$$

Note that the free components (entry) are chosen to be $w_2 = \frac{1}{A_1+A_2}$ and $v_2 = 1$ respectively, where

$$A_1 = 1 + \left(\frac{Q_1}{Q_2} - \frac{\gamma\sigma_2}{Q_2Q_3Q_4}\left(\beta_2 + \frac{\alpha_2\beta_3}{Q_5} - \frac{\alpha_2n_1n_4}{Q_5n_7} - \frac{n_1n_3}{n_7}\right)\right) + \left(\frac{\gamma\sigma_2}{Q_3^2Q_4}(\beta_2 + \frac{\alpha_2\beta_3}{Q_5} - \frac{\alpha_2n_1n_4}{Q_5n_7} - \frac{n_1n_3}{n_7})\right)$$

$$+ \frac{1}{Q_3Q_4^2}\left(\sigma_2\gamma\beta_2 + \frac{\alpha\beta_3\sigma_2\gamma}{Q_5} - \frac{\alpha_2n_1n_4\sigma_2\gamma}{n_7} - \frac{n_1n_3\sigma_2\gamma}{n_7}\right),$$

and

$$A_2 = \left(\frac{\beta_3}{Q_5} - \frac{n_1n_4}{Q_5n_7}\right)\left(\frac{\alpha_1\sigma_1}{Q_2Q_5} + \frac{\alpha_2\sigma_2\gamma}{Q_3Q_4Q_5}\right) + \frac{n_1}{n_7^2}\left(\frac{n_2\sigma_1}{Q_2} + \frac{n_3\sigma_2\gamma}{Q_3Q_4} + \frac{\alpha_1\sigma_1n_4}{Q_2Q_5} + \frac{\alpha_2\sigma_2\gamma}{Q_3Q_4Q_5}\right),$$

so that, $\mathbf{v} \cdot \mathbf{w} = 1$ (in line with [12]).

It can be shown, by computing the non-zero partial derivatives of $f_i(i = 1, ..., 9)$, that the associated bifurcation coefficients, A and B, are given, respectively, by

24

$$A = \sum_{k,i,j=1}^{9} v_k w_i w_j \frac{\partial^2 f_k(0,0)}{\partial x_i \partial x_j} = \frac{2(b - \mu_r)[(-a_1 a_2 \mu_h + a_3)v_2 + v_9 w_8 \Pi_h a_4]K - 2v_9 w_9^2 \beta_8 b \Pi_h}{\Pi_h K (b - \mu_r)},$$

$$B = \sum_{k,i=1}^{9} v_k w_i \frac{\partial^2 f_k(0,0)}{\partial x_i \partial \beta_1} = v_2 w_3,$$

where $a_1 = w_3 \beta_1 + w_5 \beta_2 + w_6 \beta_3$, $a_2 = w_2 + w_3 + w_4 + w_5 + w_6 + w_7$, $a_3 = w_1 w_9 \beta_4 \Pi_h$, and $a_4 = w_5 \beta_6 + w_6 \beta_7 + w_3 \beta_5$.

Since $v_2 > 0$ and $w_2 > 0$ imply that $B > 0$, hence we have forward bifurcation if and only if $A < 0$ (see Figure A1 for illustrative purpose) and backward bifurcation when $A > 0$. Thus, the LHF model (2.1) exhibits the phenomenon of forward bifurcation, which occurs at $\mathcal{R}_0 = 1$. If $\mathcal{R}_0 < 1$ then no endemic equilibrium appears and the disease-free equilibrium is the only local attractor. But if $\mathcal{R}_0 > 1$ then the endemic equilibrium exists. For this reason, there is a forward bifurcation because in the neighborhood of the bifurcation point, the disease prevalence is an increasing function of $\mathcal{R}_0$ (see Figure A1) which implies that the LHF model (2.1) exhibits a forward bifurcation.

A2 Sensitivity analysis

Following previous studies [27, 72, 73], we adopted the partial rank correlation coefficient (PRCC) for sensitivity analysis. The PRCC of the $\mathcal{R}_0$ of the model (2.1) is estimated. The sensitivity analysis results in Fig A2 reveal the top ranked parameters to be emphasized in controlling the LHF epidemics (i.e., rodent-to-human transmission rate β_4, maximum growth rate of the rodents K, and rodent natural death rate μ_r).

A3 Sub-exponential fitting results

We fitted the LHF cumulative number of cases at time t, with sub-exponential growth formulation adopted from [13, 14]. The parameter r (which is positive) represents the growth rate with units of people^{1-p} per unit time. Here, the p is dimensionless and we have $p \in [0, 1]$, which represents the deceleration of growth parameter. The function of this sub-exp fitting can be found in [13, 70, 71].

The parameter $A = C_0^{(1-p)}$, where C_0 is the initial case, and p is the parameter that indicates how close this "sub-exponential" to exponential. When $p = 1$, then it becomes an exponential growth rate.
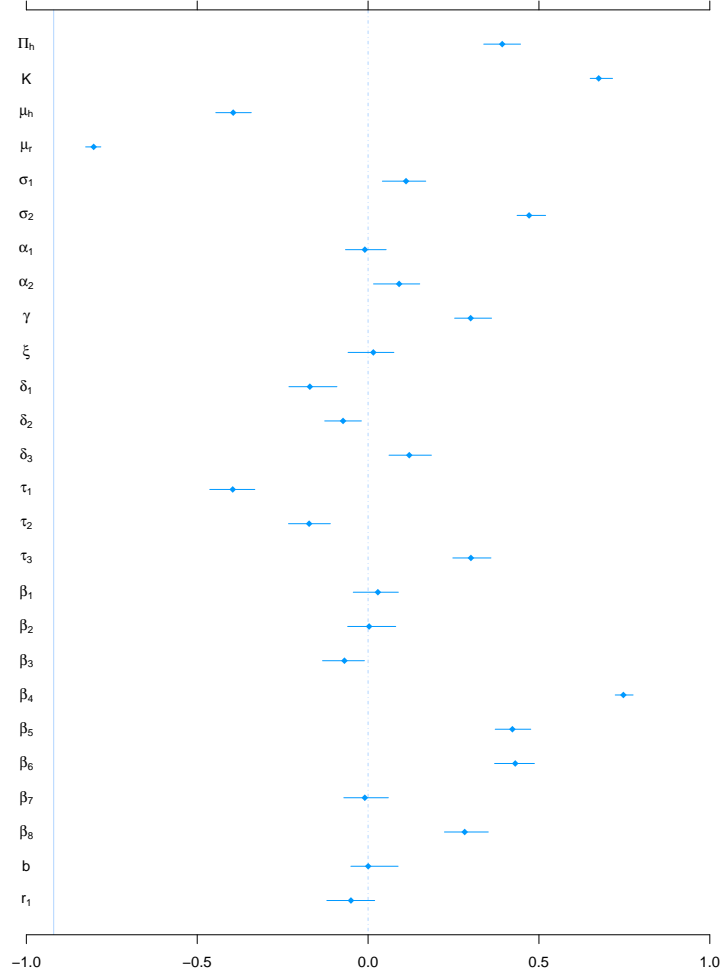
Figure A2: The PRCC of $\mathcal{R}_0$ against model parameters.
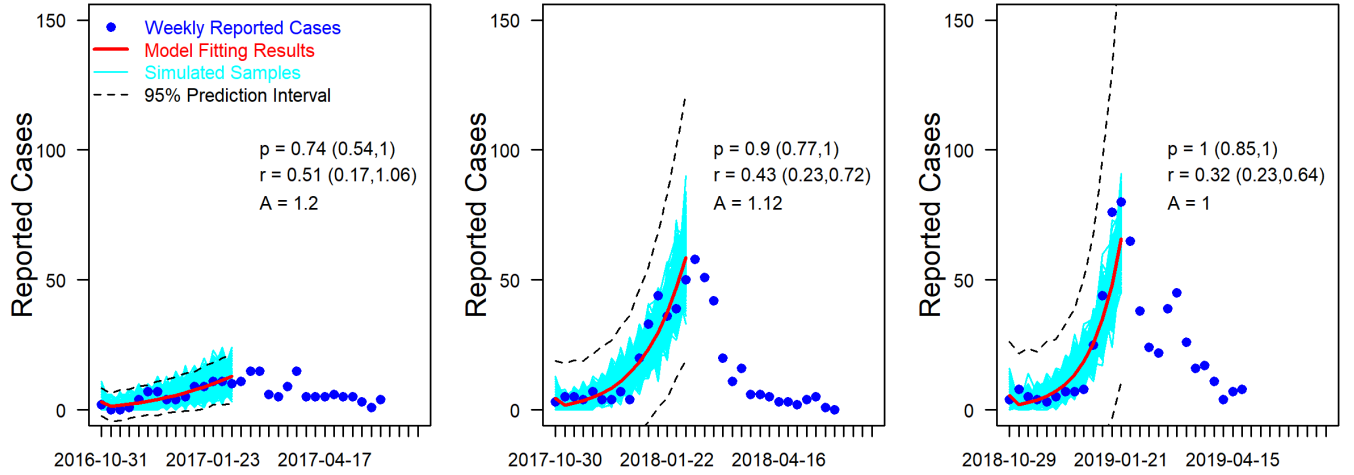
Figure A3: Fitting results of the LHF cumulative number of weekly reported cases at time t, with sub-exponential growth formulation. r denotes the growth rate, $p \in [0,1]$ represents deceleration of growth parameter with 95% CIs in the brackets and A is the constant initialization.